X-ray photoelectron-spectroscopy study of oxides of the transuranium elements Np, Pu, Am, Cm, Bk, and Cf†

B. W. Veal, D. J. Lam, H. Diamond, and H. R. Hoekstra
Argonne National Laboratory, Argonne, Illinois 60439
(Received 23 September 1976)

Systematic x-ray photoelectron spectroscopy (XPS) measurements are reported for both core and valence electrons for oxides of the actinides thorium, uranium, neptunium, plutonium, americum, curium, berkelium, and californium. The XPS spectra of the localized $5f$ electron states were compared to the appropriate multiplet calculations for the neutral atom. Agreement between theory and experiment was generally good but substantial solid-state broadening of the oxide spectra limited the capability for comparing detailed spectral features. Binding energies of several prominent core lines are systematically presented as a function of atomic number for the series of actinide oxides. Comparisons are made between the measured energies and the corresponding calculated energies reported by other investigators. Anomalous core-level spectra (most notably the $5d$'s), which probably result from coupling of the hole-state magnetic moment with the moment of the unfilled $5f$ shell, are presented.

I. INTRODUCTION

The actinide series of elements, because of their scarcity and extreme radioactivity, have received relatively little scientific attention. For the heavier actinides ($Z > 97$), studies must be performed on samples of microgram quantities or less. Furthermore, the samples may have half-lives measurable in days. However, the actinide series, with its partially filled $5f$ shell, contains a wealth of information about the physics of electrons in solids.[1]

Numerous papers have been published reporting x-ray-photoelectron-spectroscopy (XPS) spectra for compounds of uranium, the heaviest of the naturally occurring elements. In addition to the *core-level studies* which are valued for their chemical-bonding information, the $5f$-electron spectrum in uranium oxides[2-4] has also been studied previously. The $5f$ spectrum of UO_2 is simple, as expected from the f^2 configuration of the uranium ions, and its intensity can be dramatically modulated by varying the oxidation state of uranium.[3] To our knowledge, however, only Novakov and Hollander[5] and Krause and co-workers have reported XPS studies for the transuranium elements. Krause *et al.*[6] reported spectra for $Am(OH)_3$ and have measured spin-orbit splittings of the $4f$ levels in a series of actinide fluorides and oxides.[7]

Other measurements of core-level binding energies for heavy actinides have been obtained with x-ray and internal-conversion spectroscopy.[8] Agreement between these reported binding energies and the results presented in this paper are generally good (usually within the specified error limits) except for the $6p$ levels. The close proximity of the $6p$ levels to the O $2s$ and to the valence-band structure probably has led to confusion in identifying those spectral lines. The earlier studies of uranium $6p$ levels[9,10] have provided the groundwork for clear identification of the $6p$ levels in the heavier actinides. Exhaustive tabulations and comparisons of published core-level binding energies are presently being compiled and critically examined by other investigators.[11,12]

In this paper we report XPS studies on a series of oxides of the actinides neptunium through californium. Oxides tend to be stable and are often not seriously affected by exposure to air. Data were acquired from thin-film samples prepared in microgram quantities, with all samples having been exposed to air before measurement. Except for californium, an effort was made to produce dioxides of all the actinide samples but the small sample size did not permit an independent measurement of the actual oxidation state. Because of the preparation and characterization limitations, this paper must be regarded as a preliminary study of the electronic properties of actinide oxides using the XPS technique.

Binding energies of prominent core levels with energies less than 1000 eV are systematically reported for the oxide series. These data provide the first reported measurements of some of the actinide core-level energies. Within experimental error, the binding energies of the $6p$ core levels vary linearly with atomic number. The $4d$ and $4f$ levels show the same monotonic but nonlinear dependence on Z. Both the $5p$ and $5d$ levels are anomalous; the usual spin-orbit-split components are not observed for these core levels.

The XPS spectra in the valence-band region are dominated by $5f$-electron emission. The localized electrons of the partially filled $5f$ shell generate a photoemission spectrum which is believed to measure the multiplets in the excitation spectrum of the $(n-1)$-electron state of the system. (For lanthanide elements and compounds, studies of the XPS $4f$ multiplet structure,[13] have met with remarkable success. The observation of interconfiguration fluctuations in lanthanides, an extension of the multiplet studies, has also been reported.[14]) The shapes of the $5f$ electron "bands" were compared with the final-state multiplet structure of the appropriate $5f^n$ configuration. Because the oxides are insulating or semiconducting, phonon broadening[15-17] limits the spectral resolution, destroying detail which might be observable in metallic samples. Within the resolution limitations, however, generally satisfactory agreement is found between experiment and the results of the final-state multiplet theory.

II. EXPERIMENTAL PROCEDURE

The XPS spectra were obtained with a Hewlett-Packard 5950A spectrometer using monochromatized aluminum $K\alpha$ x rays. The instrument, having a resolution capability of ~0.55 eV, is equipped with a low-energy electron flood gun that is used for neutralizing the surface charge that builds up on insulating samples during the measuring process.

The ThO_2 was a thin film grown on a thorium metal substrate.[4] After sputtering with argon ions, the underlying metal spectra could be observed superimposed on the oxide spectra. The oxide lines were then referenced to the Fermi level of the metal. For UO_2, the spectra were referenced to the U $4f_{7/2}$ level taken to be 379.6 eV as measured by Verbist *et al.*[2] using the gold-decoration technique.

The remaining samples were prepared by oxidation of thin films deposited onto platinum substrates with an isotope separator. The films of most of the actinides were produced in the following way[18]: The actinide was dissolved in nitric acid and the solution was evaporated onto quartz wool and placed in the oven of the isotope separator. There it was converted to the chloride with $CHCl_3$ and volatilized into an electron plasma where the actinide +1 ion was produced and extracted. The magnetically selected mass emerges with 50–80 keV, and normally is focused to a 2-mm spot on a target foil. The ion beam can be swept vertically by varying the potential producing a 2-mm-wide line. The selected mass position on the target was replaced by a 2-mm gap behind which the platinum foil collector was oscillated laterally by a battery-driven motor to give an evenly distributed rectangular film deposit. The collector was given a retarding potential with respect to the target slit so that the ion arrived at 80 to 160 eV and did not penetrate deeply into the collector surface. The films were ~30 Å thick covering an area of 3×7 mm, only slightly larger than the size of the incident XPS x-ray beam impinging on the sample. The actinide metal films were subsequently heated in oxygen to produce dioxides (Table I).

The californium samples were prepared by volatilization from a tantalum filament onto a platinum receiver. The filament had been precleaned by heating in vacuum (~10^{-6} Torr) at white heat for several minutes. Thermal cleaning cycles were repeated until no pressure surge was detected. A drop of nitric acid solution containing 10–15 μg of californium, whose final purification step was an HDEHP (di-2-ethylhexylorthophosphoric acid)[19] column, was placed on the filament. The solvent was then evaporated in air with a heat lamp. Volatile impurities were subsequently removed from the residue by cyclicly heating it to 900–1000° C in vacuum for ~1 min. Again the temperature was cycled until no pressure surge was observed on heating. A 20-sec flash evaporation at white heat then transferred the californium to the platinum receiver. The film sample was subsequently oxidized (see Table I). No tantalum was observed in the XPS spectra.

Berkelium was separated from its californium decay product by a reversed-phase extraction chromatography (HDEHP) column,[19] and a sample was immediately prepared with the isotope separator. The time between the separation from californium to the acquisition of XPS spectra was less than a day.

Because of the extremely small amount (1–4 μg) of material used, no x-ray diffraction patterns were obtained to ascertain the crystal structure of the oxides studied. Samples of heavier actinide oxides (americium and curium) were prepared using different procedures in an attempt to produce both dioxides and sesquioxides, but the XPS spectra obtained from the oxides of a given material are similar.

Because the films were thin and of small area, weak platinum $4f$ lines from the substrate could usually be observed. These lines are by far the strongest in the platinum spectrum. Except for AmO_2 and the californium oxides, no significant perturbation of the actinide valence band data is caused by the presence of the weak platinum signal. The presence of the platinum $4f$ signal, however, provides a useful calibration line for deter-

TABLE I. Samples used in this study.

Nuclei	Half-life (principal mode of decay)	Chemical treatment	Chemical form	Ref.
^{232}Th	1.405×10^{10} yr (α)	•••	ThO_2	a
^{238}U	4.49×10^{9} yr (α)	•••	UO_2	a
^{237}Np	2.14×10^{6} yr (α)	Heated to 820 °C in air	NpO_2	b
^{242}Pu	3.87×10^{5}yr (α)	Heated to 540 °C in air	PuO_2	c
^{243}Am	7400 yr (α)	Heated to 830 °C and slowly cooled in oxygen	AmO_2	d
^{248}Cm	3.7×10^{5} yr (α)	Heated 18 h at 360 °C in 1 atm of O_2	CmO_2	e
^{249}Bk	314 day (β)	Heated to 900 °C and brought to room temperature in 1 atm of O_2	BkO_2	f
^{249}Cf	352 yr (α)	Heated in air for 90 min at 500–540 °C	Cf_7O_{12}	g
		Heated the Cf_7O_{12} sample at ~750 °C for 1 h in $\frac{1}{2}$ atm of hydrogen	Cf_2O_3	h

[a] B. W. Veal and D. J. Lam, Phys. Rev. B 10, 4902 (1974).
[b] C. Keller, *The Chemistry of the Transuranium Elements* (Kernchemie in Einzeldarstellunger, Vol. 3) (Verlag Chemie *GmbH*, Weinheim/Bergstr., Germany, 1971), p. 274.
[c] Reference b, p. 380.
[d] T. D. Chikalla and J. L. Eyring, J. Inorg. Nucl. Chem. 30, 138 (1968).
[e] W. C. Moseley, J. Inorg. Nucl. Chem. 34, 539 (1972).
[f] R. D. Baybarz, J. Inorg. Nucl. Chem. 30, 1769 (1968).
[g] R. P. Turcotte and R. G. Haire, Report No. BNWL-SA-5334, 1975 (unpublished), p. 7.
[h] R. D. Baybarz, R. G. Haire, and J. A. Fahey, J. Inorg. Nucl. Chem. 34, 557 (1972).

mining absolute binding energies of the oxides (insofar, at least, as binding energy measurements on insulating or semiconducting samples are meaningful using this calibration technique). Good electrical contact between the sample and substrate was usually maintained. Relative to the "zero-flood" condition, a charge shift less than 0.3 eV was observed (except for CmO_2) when the electron "flood gun" was used at maximum output current and zero voltage bias. Only curium oxide samples showed a charge shift greater than 0.2 eV. One (apparently) heavy film of curium oxide showed a charge of 1.0 eV but no platinum core lines were resolved. When a shift was observable, the oxide spectrum was taken as the average of the flood gun "off" and "on" positions. This procedure was used since both the flood "off" and flood "on" conditions should represent extremes of sample surface charge, with the "off" position corresponding to a positively charged surface (relative to the spectrometer ground) and the "on" position corresponding to a negatively charged surface. One would thus expect the accuracy of the binding energy measurements to be ~0.5 eV. This statement of accuracy is addressed only to the surface charging problem and not to the solid-state problems encountered with insulating or semiconducting samples. For example, the location of the Fermi level within the band gap might be determined by the kind and quantity of dopant and, for heavy (but unknown) dopings, binding energy uncertainties as large as the width of the band gap might be encountered.[20]

The oxides of neptunium, americium, berkelium, and californium were thus referenced to the substrate platinum $4f_{7/2}$ line taken to be 71.3 eV, a value measured relative to the Fermi edge of the metal. The plutonium and curium oxide samples were not measured absolutely because for these samples a suitable platinum reference line was not obtained. For these samples, the core line binding energies were referenced to the Pt $4f_{7/2}$ line measured in a separate run (i.e., the spectrometer was calibrated against the platinum line). It was noted that for ten experiments involving the actinide oxides (and platinum metal), that the spectrometer calibration was reproducible to better than 0.5 eV. For CmO_2, an additional charge shift correction, as discussed above, was imposed.

The spectra shown in this paper originate from samples that have been treated to produce the dioxides (except the californium oxides) as outlined in Table I. However, irradiation by aluminum

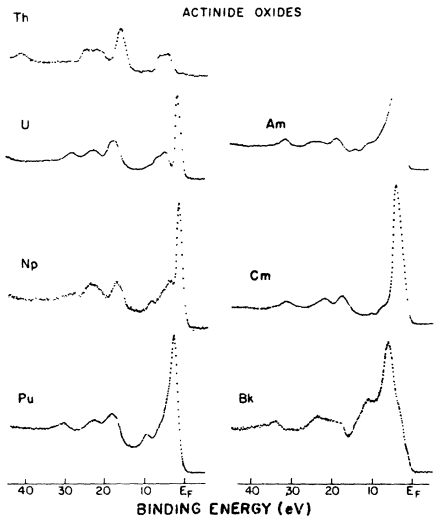

FIG. 1. XPS spectra for oxides of the actinides thorium and berkelium within 50 eV of the Fermi level. The prominent features near E_F result from $5f$-electron excitations. The weak shoulder in AmO_2 appearing near E_F is a superimposed signal from the platinum substrate.

$K\alpha$ x rays and sample heating (over 100 °C) in vacuum during the course of the measurements may have reduced some of the samples. (We have observed this effect in UO_3 and U_3O_8.) Radiation from the 314-day ^{249}Bk or 352-yr ^{249}Cf nuclei might also have a small effect on sample composition.

Only preliminary data are now available for oxides of californium. These data include some of the core lines but not the valence-band results. No attempt was made to produce CfO_2 since the dioxide is likely to be reduced in the measurement process (see Sec. III B). Samples of Cf_2O_3 and Cf_7O_{12} were prepared but, in all cases, strong contaminant lines were observed. Also, strong superimposed platinum signals from the substrate severely limits the usefulness of the valence-band data.

III. RESULTS AND DISCUSSION

A. Core-level spectra

Figure 1 shows the XPS spectra, within 50 eV of the Fermi level, for the oxides presently investigated as well as the spectra of ThO_2 and UO_2 which were previously published.[4] The three-peak structure centered around 25 eV is apparent in each of the oxides. These peaks are the actinide $6p_{1/2}$, O $2s$, and actinide $6p_{3/2}$ lines, respectively. The $6p$ core levels do not increase in binding energy with atomic number sufficiently rapidly to affect any change in the ordering of these levels for the entire series of oxides. In ThO_2, at the lowest binding energy, only the O-$2p$-derived bonding electrons are observed. In UO_2, a peak resulting from two localized $5f$ electrons appears between the O $2p$ electrons and the Fermi level E_F.[4] For the heavier oxides, which contain increasingly larger numbers of occupied $5f$ electrons, the intensity of the outermost ($5f$) peak (the peak nearest E_F) grows substantially relative to the actinide $6p$'s or the O $2s$ peak. The $5f$ spectrum also moves toward higher binding energy relative to the oxygen lines with increasing atomic number. Furthermore, for increasing Z, the $5f$ spectrum acquires more structure and experiences varying degrees of linewidth. These features result from the presence of multiplets in the XPS "final-state" spectra. These effects will be discussed in Sec. III B.

The "absolute" binding energies of several prominent core lines were also measured for the oxide series. Figure 2 shows the systematic dependence of these binding energies on atomic number. The results are also tabulated in Table II. For completeness ThO_2 and UO_2 are also included.

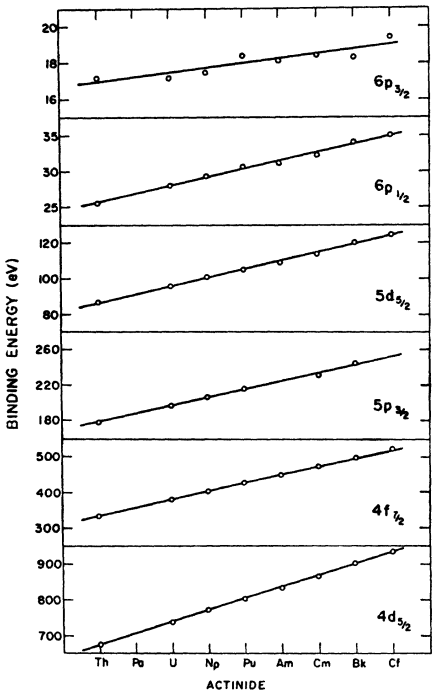

FIG. 2. Binding energies for several actinide core levels (measured in a series of actinide oxides) plotted as a function of atomic number. The straight lines are linear least-squares fits to the data.

TABLE II. Actinide-oxides—core-level energies (in eV).

	$6p_{3/2}$	$6p_{1/2}$	$5d_{5/2}$	$5p_{3/2}$[a]	$4f_{7/2}$	$4f_{5/2}$	$4d_{5/2}$	$4d_{3/2}$	O 2s	O 1s	C 1s
ThO_2	17.2	25.2	87.0	178.9	334.6	343.9	675.7	713.0	22.9	530.5	285.4
UO_2	17.2	28.1	96.0	197.2	379.6	390.5	737.7	780.1	22.5	529.7	284.6
NpO_2	17.5	29.3	100.9	206.3	402.5	414.3	771.2	816.1	23.8	529.7	284.5
PuO_2	18.4	30.6	105.0	216.2	426.6	439.3	801.8	849.8	22.8	530.3	285.3
AmO_2	18.1	31.1	108.4	•••	448.2	462.5	832.0	883.1	23.1	529.0	284.4
CmO_2	18.4	32.1	113.2	231.7	472.7	487.4	865.2	918.7	22.7	530.1	284.0
BkO_2	18.3	34.0	120.1	245.8	498.5	514.4	901.4	957.7	23.4	529.5	285.3
Cf_2O_3	19.4	34.9	124.5[b]	•••	523.3	541.1	933.1	993.7	24.7	530.3	283.9
							Average		23.2	529.9	284.7

[a] The high binding-energy component of the doublet.
[b] Strongest peak.

The californium data in Fig. 2 is from a sample of Cf_2O_3 (Table I). (Relative to the Cf_7O_{12} results, these data were less severely affected by sample contamination problems, particularly within 50 eV of the Fermi level.) The Cf $4f$ lines of the Cf_2O_3 were ~5 eV wide, much broader than the other actinide $4f$ lines, but were not resolvable into component lines. For Cf_7O_{12}, however, the $4f$ lines are clearly resolved, apparently into two chemically shifted sets of lines corresponding to different oxidation states. These data are shown in Fig. 3 along with $4f$ core level spectra of the other actinide oxides. The ~2.5-eV splitting of the Cf $4f$ levels is similar to the $4f$ level splitting observed in intermediate oxides of uranium.[2]

Strong satellite peaks are observed following the $4f$ levels of uranium, neptunium, plutonium, and berkelium (Fig. 3). Line-shape distortions of the americium, curium, and berkelium lines are apparent. The ratios of peak heights and widths for some spin-orbit components, particularly for the americium levels, are anomalous. The $4f$ lines of berkelium oxide show strong satellite lines ~7 and 10 eV from the main peaks. These shifts are too large to correspond to chemical shifts for the different oxidation states (between UO_2 and UO_3, shifts of ~1 eV are seen).[2] In general, the strong satellite structure, the lineshape distortions, and anomalous spin-orbit splittings are not readily understood.

In Fig. 2 and Table II, core level energies are also presented for the $5p_{3/2}$ and $5d_{5/2}$ levels. Since the spectra with principal quantum number $n=5$ tend to be complex, we have not included the $j=l-s$ spin-orbit component. The $5d_{5/2}$ level is taken to be the strongest (highest-intensity) peak of the $5d$ complex. Except for Cf_2O_3, this peak also has the lowest binding energy of the complex. These core level spectra presumably show multiplet effects associated with spin coupling between the hole state and unpaired $5f$ valence electrons. Such spin pairings are believed to be strongest for electrons of the same principal quantum number as the unfilled valence electrons.[21] Figure 4 shows examples of $5d$ spectra for several of the actinide oxides. Only for ThO_2, which has no $5f$ electron occupation, is the $5d$ spectra "normal." The weak shoulders on the low binding-energy sides of the ThO_2 peaks are weak signals from the underlying metal. For all of the other oxides, one cannot clearly identify the usual spin-orbit-split components. The most prominent secondary peak (normally the $d_{3/2}$ peak) is so distorted, attenuated, or broadened, that its binding energy difference from

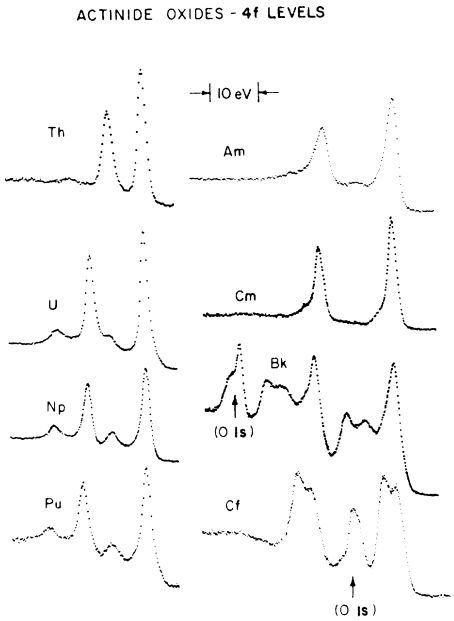

FIG. 3. Actinide $4f$ core-level spectra recorded for oxides of the elements thorium through californium.

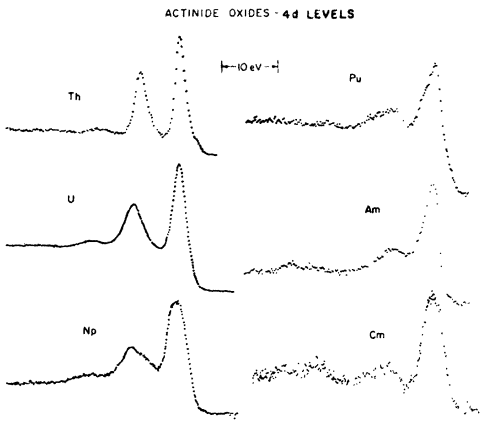

FIG. 4. Actinide 5*d* core-level spectra recorded for oxides of the elements thorium and curium. The $d_{3/2}$, $d_{5/2}$ spin-orbit components cannot be recognized in the heavier elements.

the $d_{5/2}$ line must be a very poor measure of the actual spin-orbit interaction. These results are reminiscent of the 4*d* core-level line shapes for the lanthanide series elements where very complicated structures resulting from multiplet splittings were observed.[22]

Figure 5 shows the Pu $5p_{3/2}$ core level. This doublet line is very similar to the $5p_{3/2}$ level that was studied in a series of uranium compounds.[10] It was established that the unusual structure in the $5p_{3/2}$ peak was relatively insensitive to chemistry (little change was seen between U^{4+} and U^{6+} samples). Interestingly, the $5p_{3/2}$ levels continue to show the same characteristic doublet structure for all of the actinide oxides (uranium through berkelium) with the possible exception of the americium and californium oxides. For these samples, we suspect that additional distortion results from the

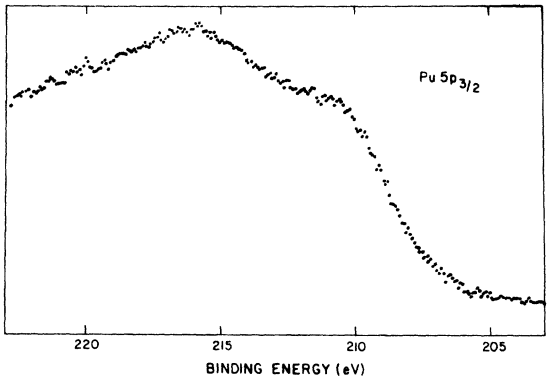

FIG. 5. Pu $5p_{3/2}$ core level measured in PuO_2. This doublet structure appears to be characteristic of the $5p_{3/2}$ line for all of the actinides.

superposition of surface impurity lines. Thus these $5p_{3/2}$ lines were not included in Table II or Fig. 2.

It is satisfying that the calibration procedures produce a monotonic sequence of core-level binding energies spanning eight samples. In order to enhance the sensitivity in the display of the systematics of the core-level energies, linear least-squares lines were fit to the actinide core-level data of Fig. 2. Figure 6 shows the deviations between the experimental 4*d*, 4*f*, and 6*p* data and the corresponding linear fits (ΔE). For the low binding-energy 6*p* levels, there is no detectable deviation from linearity with *Z*. For the 4*d* and 4*f* core levels, however, a significant deviation from linearity is observed in the sequence. Also shown in Fig. 6 (dashed lines) are the deviations from a linear fit (chosen to pass through uranium and berkelium) to the self-consistent-field relativistic Hartree-Fock-Slater results calculated by Carlson *et al.*[23] for the $4f_{7/2}$ and $6p_{3/2}$ levels. Only calculations for a sequence of elements having a systematic change in the $5f^n$ configuration with *Z* are presented. The sequence here represents the $6d^1 5f^n$ sequence (a fixed *d* electron concentration and varying 5*f* concentration) which was computed for the elements actinium, protactinium, uranium, neptunium, curium, berkelium, and fermium. (A shift of about 5 eV at a given *Z* is seen between the 4*f* binding energies computed for the $d^1 f^n$ sequence and for the $d^0 f^n$ sequences but the systematic behavior of the two sets of calculations is very similar.) The dashed lines in Fig. 6(a), representing the neutral atom calculations for the $4f_{7/2}$ lines, shows the same general systematic beha-

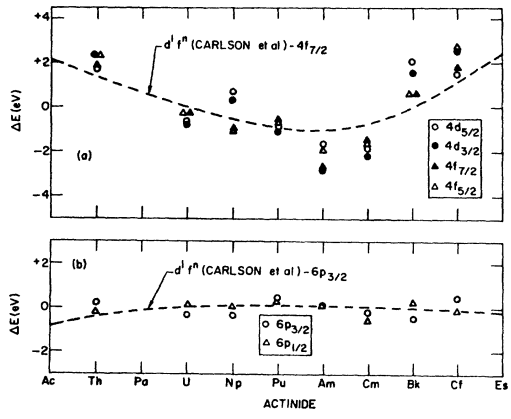

FIG. 6. Deviations between measured core-level energies and corresponding linear fits to those energies (see Fig. 2) plotted against atomic number. The dashed lines are deviations from a linear fit to the theoretical results of Carlson *et al*. (Ref. 23) for the $4f_{7/2}$ and $6p_{3/2}$ levels.

vior as is observed experimentally. Furthermore, only a very weak (and opposite) curvature is seen for the low-lying $6p$ levels [Fig. 6(b)] which is again consistent with the experimental observations.

Presenting the data and computed results in this way helps to account for the experimentally observed curvature in the binding-energy–atomic-number plots and tends to reinforce confidence in the calibration procedures, but does not provide a very demanding test of the theory. It is instructive to examine the tabulated experimental and theoretical binding energies for the $j=l+s$ lines listed in Table III. This table contains the results of Carlson *et al.*[23] and Desclaux[24] for the neutral atom and the results of Desclaux and Freeman[25] for the actinide 4+ ions.

The calculations of Carlson *et al.* are based on the self-consistent-field Hartree-Fock-Slater method where relativistic effects are handled as perturbations on the nonrelativistic Hartree-Fock results. Exchange is approximated according to the method of Slater. The values reported by Desclaux were obtained with a self-consistent-field method by solving the Dirac-Fock equations using a configuration averaged potential. Relativistic effects and exchange are included without approximation.

The binding energies of Carlson *et al.* are generally within 10 eV of experiment, certainly a reasonable discrepancy considering that our measurements are taken for solid (and insulating or semiconducting) samples, whereas the calculations pertain to the free atoms. An offset correction to the theoretical results would improve agreement with the lower binding-energy levels but would not improve agreement with the deepest levels, the $4d$'s. For the low binding-energy levels, the free-atom results of Desclaux differ by about 10 eV from experiment and by 25–30 eV for the deeper levels. The noticeably nonsystematic dependence of theoretical core-level energies on Z (Table III) results from the nonsystematic choice of configuration change with Z as discussed above. The "U-Cm" entry in Table III represesents the binding energy differences for a given core line for uranium and curium, and indicates the slope of binding energy with Z. (Uranium and curium were chosen because d^1f^n configurations were used by both Carlson *et al.* and Desclaux for these elements.) For all core lines, the theoretical slopes are higher than are observed experimentally. Table III also includes calculated results of Desclaux and Freeman for the actinide 4+ ions (the entries in parentheses are extrapolated), which might be expected to produce better agreement with experiment than the free atom results.

TABLE III. Binding energies—experimental and theory.

	Expt.	Atom [a]	Atom [b]	4+ ion [c]
		$6p_{3/2}$		
Th	17.2	24.80	27.27	
Pa	•••	23.64	25.98	
U	17.2	24.37	26.80	61.08
Np	17.5	25.03	27.52	62.41
Pu	18.4	23.28	25.57	63.66
Am	18.1	23.78	26.04	64.83
Cm	18.4	26.72	29.38	(65.92)
Bk	18.3	27.24	26.89	
Cf	19.4	25.06	27.27	
U-Cm	1.02	2.35	2.58	(4.84)
		$5p_{3/2}$		
Th	178.9	189.15	204.27	
Pa	•••	193.76	210.15	
U	197.2	202.97	220.22	258.30
Np	206.3	212.05	230.11	268.82
Pu	216.2	215.88	235.13	279.24
Am	•••	224.80	244.62	289.59
Cm	231.7	239.00	259.35	(299.90)
Bk	245.8	248.04	263.55	
Cf	•••	251.41	273.02	
U-Cm	34.8	36.03	39.13	(41.60)
		$4d_{5/2}$		
Th	675.7	676.04	704.83	
Pa	•••	702.49	732.79	
U	737.7	734.28	765.48	803.56
Np	771.2	766.29	798.33	837.02
Pu	801.8	793.08	826.47	870.71
Am	832.0	825.68	859.57	904.67
Cm	865.2	864.20	898.47	(938.94)
Bk	901.4	897.65	926.75	
Cf	933.1	925.48	960.85	
U-Cm	127.5	129.92	132.99	(135.38)
		$5d_{5/2}$		
Th	87.0	96.71	101.19	
Pa	•••	97.95	103.70	
U	96.0	103.48	109.98	147.62
Np	100.9	108.84	116.11	154.39
Pu	105.0	109.19	117.72	161.04
Am	108.4	114.32	123.44	167.62
Cm	113.2	124.44	134.00	(174.18)
Bk	120.1	129.61	134.77	
Cf	124.5	129.31	140.40	
U-Cm	17.3	20.96	24.02	(26.56)
		$4f_{7/2}$		
Th	334.6	347.99	358.56	
Pa	•••	366.23	378.22	
U	379.6	389.79	402.52	440.86
Np	402.5	413.50	426.94	465.89
Pu	426.6	431.89	446.61	491.10
Am	448.2	456.05	471.16	516.52
Cm	472.7	486.11	501.41	(542.18)
Bk	498.5	510.98	521.04	
Cf	523.3	530.13	546.40	
U-Cm	93.3	96.32	98.89	(101.32)

[a] Carlson et al. (Ref. 23).
[b] Desclaux (Ref. 24).
[c] Freeman (Ref. 25).

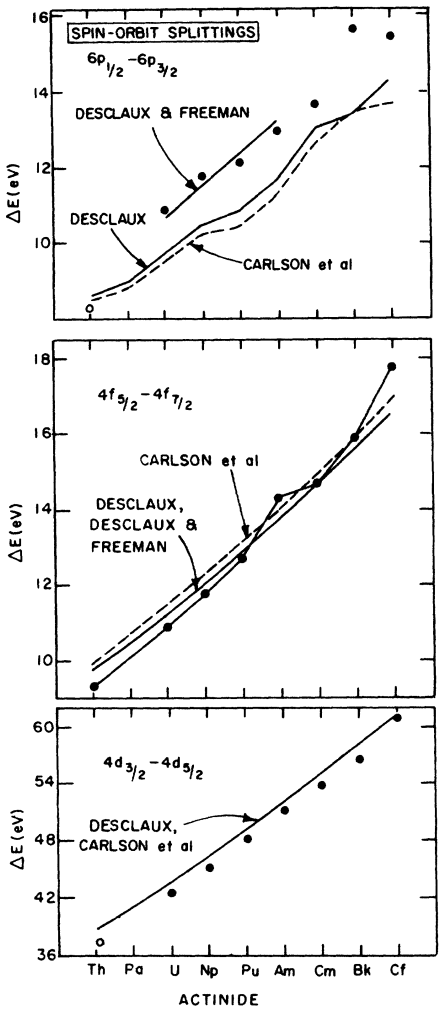

FIG. 7. Spin-orbit splittings of $6p$, $4f$, and $4d$ core levels for the series of actinide oxides shown with neutral atom theoretical results of Desclaux (Ref. 24) and Carlson *et al.* (Ref. 23) and with the 4+ion results of Freeman (Ref. 25).

However, the experimental binding energy versus Z slopes are closer to the free-atom results, particularly those of Carlson *et al.*

The measured spin-orbit splittings for the $6p$, $4f$, and $4d$ levels are shown in Fig. 7. The spin-orbit splittings of the $4f$ lines are in good agreement with the results of Krause[6,7] who showed that this rather anomalous sequence does not result from chemical shifts. Krause obtained comparable results for actinide fluorides and oxides. The theoretical results of Desclaux and of Carlson *et al.* are shown for comparison. For four of the samples, uranium through americium, calculations by Desclaux and Freeman, for the actinide 4+ ions[25] are also shown in Fig. 7. These results differ significantly from those of Desclaux and of Carlson *et al.* for the $6p$ levels and more nearly correspond to experiment. (Again the apparent scatter in the calculated $6p$ splittings results from the nonsystematic way in which the outer electron shells are filled. The sequences d^2f^n, d^1f^n, and d^0f^n are all represented.) For the spin-orbit splittings of the $4d$ levels, all of the theoretical results[23,24] are in essential agreement but are ~1 eV larger than the experimental values.

Figure 8 shows the O 1*s* lines for the sample series. The values listed in Table II are for the low binding-energy components when the O 1*s* lines are composite. The high binding-energy component of the doublet structure observed for several of the samples may result from sample surface contamination since it appears to be more sensitive to variations in sample treatment and is generally less reproducible.

Within scatter, both the O 1*s* and O 2*s* lines are constant (see Fig. 9) for the series of actinide oxides and have average values of 529.9 and 23.2 eV, respectively. Nefedev *et al.*[26] have tabulated the O 1*s* binding energies of a series of lanthanide sesquioxides. These results show a small (~0.6 eV) but roughly monotonic binding energy increase with atomic number for the series. Our results are not sufficiently precise to discern any such correlation. (A linear least-squares fit shows less than 0.1 eV increase in the binding energy with increasing Z for the series of actinide oxides.)

The low binding-energy C 1*s* contaminant peak

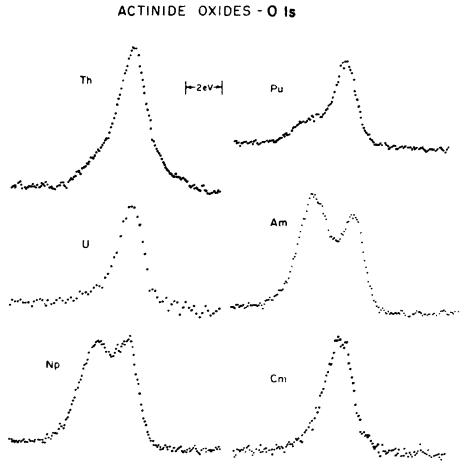

FIG. 8. O 1*s* lines observed in oxides of the actinides thorium through curium. High binding-energy components (to the left of the figures) are believed to result from surface contamination. The O 1*s* lines for the berkelium and californium oxides appear close to the actinide $4f$ lines (see Fig. 3).

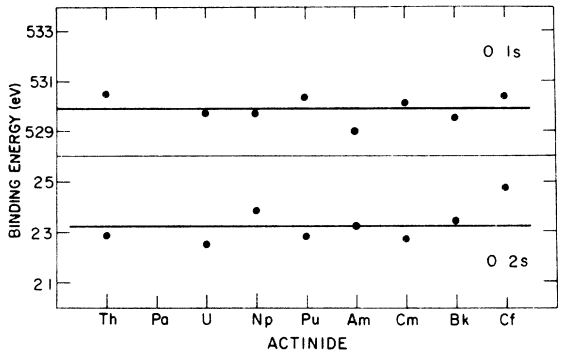

FIG. 9. Measured binding energies of the O 1*s* and O 2*s* lines for the series of actinide oxides. For the O 1*s* line, only the low binding energy component was recorded if the line showed composite structure. Constant values of 529.9 and 23.2 eV, respectively, were obtained for the O 1*s* and O 2*s* lines for the oxide series.

was measured for the oxide series along with the actinide and oxygen core levels and is also presented in Table II and Fig. 10. Within scatter, this level is constant for the entire series of oxides. Although significant scatter is observed, this result lends some support to the frequently used argument that the contaminant C 1*s* line can be used for a binding-energy reference level. The average of the measured C 1*s* binding energies is 284.7 eV.

B. 5*f* electron spectra

In the localized 5*f* electron model, the XPS 5*f*-electron spectra may be understood in terms of final-state multiplet structure. An incoming photon ejects an electron and in the process, leaves the ion in any of a number of possible final states. Since these states represent different degrees of excitation of the ion, the outgoing electron will escape with kinetic energy determined by the excitation state of that remaining ion. Therefore, an energy analysis of the photoejected electrons will provide a measure of the ion multiplet spectrum.

Not all of the possible excitation states of that ion can be produced (in an electric dipole process) through the elastic emission of an electron by an incident photon. The simplest view of the excitation process is to permit the escaping electron to satisfy the electronic-dipole selection rules and to calculate the possible excitation states of the $(n-1)$-electron ion, which give nonzero overlap with the n electron ground state of the neutral atom.[27]

Before computing the overlap, a solution is needed for the perturbation

$$H_0 = H_{\text{Coul}} + H_{\text{s.o.}} + H_{\text{crystal}} \quad (1)$$

on the spectrum of the hydrogenlike (charge-Z) Hamiltonian. H_{Coul} represents the repulsive electron-electron interaction, $H_{\text{s.o.}}$ is the spin-orbit interaction, and H_{crystal} is the crystal-field interaction which, of course, affects electrons in solids.

Since *ab initio* calculations have not precisely pinpointed any of these terms in the Hamiltonian, it is more convenient to resort to optical data (transmission measurements on ions in solution) to fix suitable parameters which characterize the perturbed Hamiltonian. XPS data (sensitive to the final state) for a f^n system are thus to be analyzed with resort to optical data characterizing the excitation spectrum of the f^{n-1} atom. This procedure has successfully been applied to studies of the localized 4*f* electron spectra in lanthanide elements and compounds, including configuration-fluctuation systems.[13,14] The analyses were based on the final-state $|SL\rangle$ coupled multiplets of $4f^n$ configurations.

For localized 5*f* electrons the spin-orbit term is sufficiently large relative to the Coulomb term than an intermediate coupling scheme must be invoked. Furthermore, the spin-orbit and crystal-field terms are of comparable magnitude. Thus, the experimental XPS spectra should be compared with the final-state crystal-field multiplet structure computed in an intermediate coupling scheme. It is, however, not possible to calculate the complete crystal-field multiplet structure for the $5f^n$ configurations when the number of *f* electrons is greater than five with currently available computational capability. Thus we have compared the experimental spectra to the free-ion final-state multiplet structure using intermediate coupling as specified by the optical experiments. Inclusion

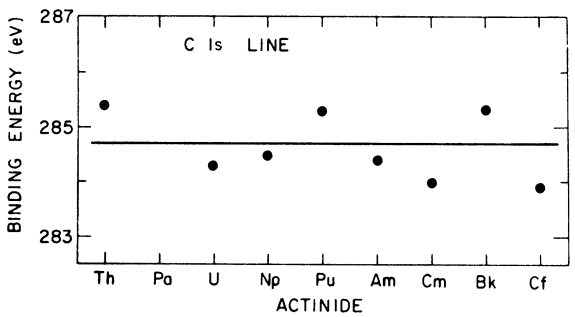

FIG. 10. Contaminant C 1*s* binding energies in the actinide oxide series. The low binding-energy component was recorded when the spectra were composite. The constant value of 284.7 eV for the series lends support to the practice of using the contaminant C 1*s* line as a calibration standard for measuring absolute binding energies.

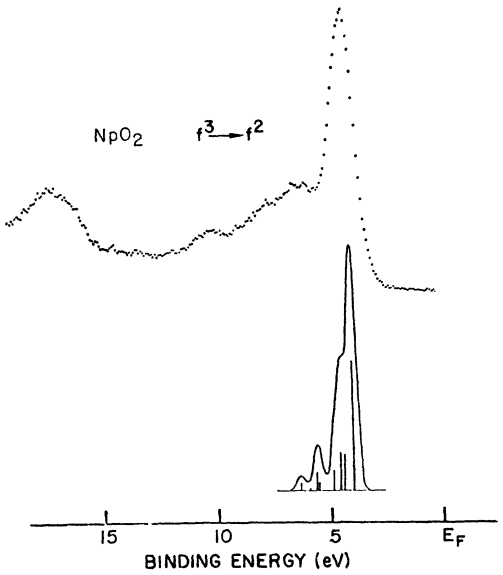

FIG. 11. Valence-band XPS spectra for NpO_2 compared with the theoretical multiplet calculation for the free-ion f^2 final state. The bonding (predominantly O $2p$) electrons contribute to the broad peak centered near 7 eV.

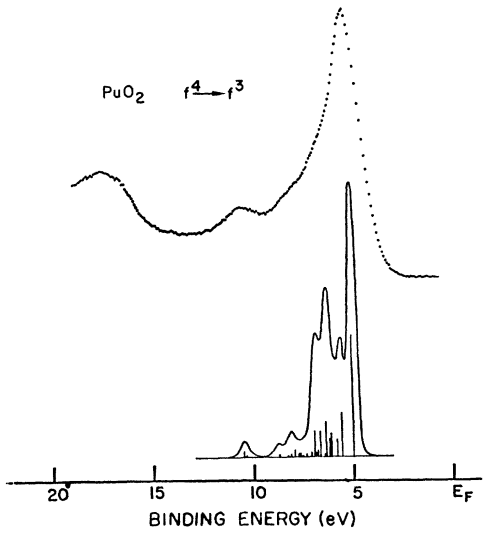

FIG. 12. Valence-band XPS spectra for PuO_2 compared with the multiplet calculation for the free-ion f^3 final state. The $5f$ electron spectra now overlap the weaker spectra from the O $2p$ electrons.

of crystal-field effects will produce additional line splittings and some modulation of the computed intensities. However, the simpler calculation should provide a good first-order determination of the multiplet spectra.

The relative intensity of each J multiplet was calculated with Eq. (A4) of Appendix A in terms of Z_f (the one electron escape probability), and the resultant multiplet structure was convoluted with a Gaussian broadening function of 0.55 eV to simulate the experimental resolution. (In these oxides, solid-state broadening effects are large so that the observed resolution is appreciably worse than 0.55 eV.) To compare with the experiments, we used the multiplet structure of the ion with one less $5f$ electron; e.g., the multiplet structure of the U^{4+} ion as the final state for the Np^{4+} ion in NpO_2, etc. An alternate choice of the final state would be the Np^{5+} ion. However, spectroscopic data are not available for all of the actinide 5+ ions. (There is no firm theoretical basis to justify the choice of one final state in preference to the other.) The experimental XPS valence spectra of NpO_2, PuO_2, and AmO_2, together with the calculated final-state multiplet structure, are shown in Figs. 11, 12, and 13. These multiplet spectra are dominated by the ground-state (atom) to ground-state (ion) transition. This (lowest binding-energy) peak was aligned with the dominant peak observed experimentally. For NpO_2, the $5f$ spectrum is not sufficiently dominant over the "bonding" (O $2p$) electrons such that a correspondence between observed structure and detail in the multiplet structure can be specified. However, for PuO_2 and AmO_2, weak experimental structure on the high binding-energy side of the $5f$ peak can be correlated with structure in the calculated multiplet spectrum. (The shoulder near E_F appearing on the

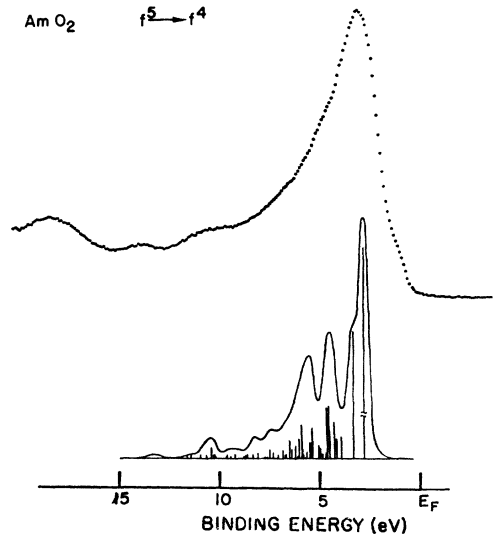

FIG. 13. Valence-band XPS spectra for AmO_2 compared with the multiplet calculations for the free-ion f^4 final state. The $5f$ electron spectra now substantially dominates the broad O $2p$ spectra. The weak shoulder near E_F results from a superimposed platinum signal from the sample substrate.

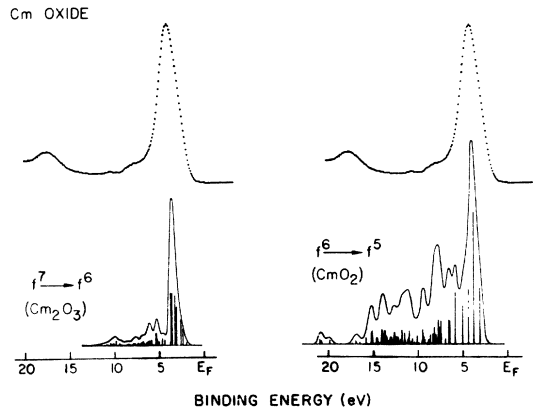

FIG. 14. Valence-band XPS spectra for a curium oxide sample. Because of the possibility that the sesquioxide (rather than the dioxide) was measured (see text), we have compared the data with both the f^6 and f^5 free-ion final-state multiplet calculations. (Note that the calculated f^6 final-state spectrum for Cm_2O_3 is based on optical data for the Cm^{4+} ion.)

valence band spectrum of AmO_2 is a signal from the platinum substrate that is superimposed on the oxide data.)

The lighter actinides from thorium through neptunium do not form stable sesquioxides and the dioxide is the lowest valence stable oxide. Beginning with plutonium, however, the actinide sesquioxides can be prepared and their stability relative to the dioxides tends to increase with increasing atomic number. Although samples were prepared in accordance with procedures designed to produce the dioxides for each of the actinides (except californium), it may be that for the heavier elements, we were actually measuring the sesquioxides or intermediate oxides. Because of this uncertainty, we have plotted, in Figs. 14 and 15, the experimental spectra for the curium and berkelium oxides along with the multiplet calculations appropriate for both the dioxides and the sesquioxides. Particularly in the case of berkelium, there seems to be good reason to suspect the sesquioxide or perhaps a mix of dioxide and sesquioxide. The possibility of a mixed oxide is difficult to confirm, however, with the core level spectra. The complex satellite structure following the *Bk* 4*f* lines, tends to mask features associated with mixed oxide phases. If, however, the weak shoulder on the high binding-energy side of the main peaks resulted from an oxidation shift, this would imply that the sesquioxide was the dominant phase. One can infer that if we have a mixed phase system, then the sesquioxide (low binding energy) must dominate over the dioxide.

There is also uncertainty about the oxidation of the curium oxide. Figure 14 shows the multiplet structure expected for the dioxide and sesquioxide. The f^6 configuration is the first (smallest f^n) configuration in the actinide oxide series for which the ground-state- (atom) to-ground-state (ion) transition does not dominate the spectrum. This leads to a skewing of the leading (low binding-energy) edge. Unlike the lighter oxides, this effect is seen in the data of Fig. 1. The two sets of multiplet spectra compared in Fig. 14 to experiment, do not clearly establish the oxidation state of the sample. However, like berkelium oxide, there appears to be a closer correspondence with experiment for the sesquioxide than for the dioxide. Again, if the high binding-energy shoulder on the 4*f* peaks were attributed to the dioxide, this would confirm the sesquioxide dominance. However, the general complexity of the satellite spectra for the 4*f* lines of the actinides makes such an interpretation dubious.

IV. CONCLUSIONS

XPS spectra for core and valence electrons in oxides of the actinides thorium, uranium, neptunium, plutonium, americium, curium, berkelium, and californium are presented. The spectra in the valence band region are predominatly determined by the 5*f* electrons which have a high photoemission cross section for 1486.6-eV (aluminum $K\alpha$) photons. Since the localized 5*f* states exist in partially filled shells, "final-state" multiplets are observed in the XPS measurement process. The observed multiplet spectra are compared with theoretical spectra whose intensities were computed using coefficients of fractional percentage [simple overlap between the n- and $(n-1)$-electron states] and whose energies were measured with

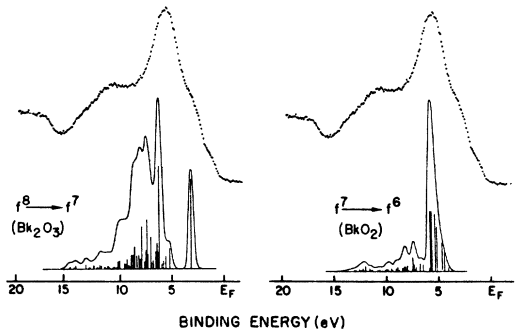

FIG. 15. Valence-band XPS spectra for a sample of berkelium oxide. For the heavier actinide oxides, there is a possibllity that the sesquioxide (rather than the dioxide) was measured (see text), so we have compared the data with both the f^7 and f^6 free-ion final-state multiplet calculations.

optical absorption spectroscopy of ions in solution. Agreement between the theoretical and experimental spectra was generally good but substantial solid state broadening of the oxide spectra ruled out the possibility of comparing detailed spectral features. Subsequent studies of pure actinide metals and intermetallic compounds should provide more detailed tests of the "final-state multiplet theory."

Binding energies of several prominent core levels were systematically recorded as a function of atomic number for the series of actinide oxides. The monotonic behavior of the core level energies for the sequence provides evidence that the calibration procedures for measuring the binding energies are reliable. Comparisons are made between measured binding energies and spin-orbit splittings, and the corresponding calculated quantities as reported by Carlson *et al*, Desclaux, and Freeman.

Some core-level spectra were anomalous in character, most notably the $5d$ levels. These data were characterized by an increasingly diffuse $d_{3/2}$ component for the heavier elements, an effect which probably results from coupling of the hole-state magnetic moment with the moment of the unfilled $5f$ electron shell.

The $5p_{3/2}$ level shows a doublet structure which appears to be characteristic of the entire actinide series. A comparable $5p_{3/2}$ line shape, found to be insensitive to chemical coordination and $5f$ electron occupation, was earlier reported for several uranium compounds.

This work represents the first systematic study of the core– and valence-electron states in transuranium materials using the XPS technique. It is expected that the XPS technique will provide significant new insights into the character of the $5f$ electrons, including their itinerant and localized behavior, and their role in chemical bonding.

ACKNOWLEDGMENTS

The authors are indebted to J. P. Desclaux and A. J. Freeman for permission to use their calculated free-ion eigenvalues prior to publication, to F. Wagner for supplying $5f$ multiplet calculations for berkelium and californium, to W. T. Carnall for stimulating discussions, and to A. P. Paulikas and J. Lerner for valuable experimental assistance.

APPENDIX A: MULTIPLET INTENSITY CALCULATION

The Russell-Saunders basis functions were used to set up matrix elements for the combined electrostatic and spin-orbit interactions of the free ion.[28] These matrix elements may be expressed in terms of only four variables, which change from element to element in the actinide series. The variables are the E^1, E^2, and E^3 of Racah[29] and the spin-orbit integral ζ_{5f}. In the present calculation, the four variables are treated as parameters derived from spectroscopic data. The entire matrix was diagonalized to give the energy levels. The eigenvectors resulting from the diagonalization are characterized by J. These are linear combinations of the various ν, S, and L components that span the manifold of constant J of an f^n electron configuration and are in the form

$$|\alpha JM\rangle = \sum_{\nu SL} \langle f^n \nu SLJM | \alpha JM\rangle | f^n \nu SLJM\rangle ,$$

where ν represents seniority and the two other quantum numbers W and ξ introduced by Racah.

The probability for photoionization from a $|\alpha JM\rangle$ initial state to a $|\alpha' J' M'\rangle$ final state may be written[27]

$$X = Z_f \sum_{M, j, m_j} |\langle \Psi^F(\alpha' J' M') | a^r_{j, m_j} | \Psi^I(\alpha JM)\rangle|^2 , \tag{A1}$$

where Z_f is the one electron cross section for the f electrons, and a^r_{j, m_j} is an annihilation operator which annihilates an f electron from the initial state. This annihilation operator may be treated[30] as an irreducible tensor operator, and its matrix elements are determined by the way in which the electrons are coupled to produce the initial $|\alpha JM\rangle$ and final $|\alpha' J' M'\rangle$ states. By neglecting the crystal-field interaction of the actinide ions in the oxide and treating the irreducible tensor operator a^r_j as an irreducible product of two tensor operators acting between the coupled states J and J', Equation (A1) can be reduced to the matrix element between the uncoupled $|\nu SL\rangle$ states using the standard $9j$ coefficient

$$X(\alpha' J') = Z_f \sum_{\substack{\nu SL \\ \nu' S' L'}} (2J'+1)(2S'+1)(2L'+1)(\langle f^{n-1} \nu' S' L' | \alpha' J'\rangle \langle f^n \nu SLJ | \alpha J\rangle)^2$$
$$\times |\langle f^{n-1}(\nu' S' L') || a^r || f^n (\nu SL)\rangle|^2 \sum_j (2j+1) \begin{pmatrix} S & S' & \frac{1}{2} \\ L & L' & 3 \\ J & J' & j \end{pmatrix}^2 , \tag{A2}$$

TABLE IV. Slater integrals and the spin-orbit parameters for the various actinide ions.

Ion	Configuration	$E^1(\mathrm{cm}^{-1})$	$E^2(\mathrm{cm}^{-1})$	$E^3(\mathrm{cm}^{-1})$	$\zeta_{5f}(\mathrm{cm}^{-1})$
U^{4+}	$5f^2$	3091.85	15.70	301.32	1870.0
Np^{4+}	$5f^3$	3362.02	17.08	327.65	2193.0
Pu^{4+}	$5f^4$	3647.19	18.52	355.44	2426.0
Am^{4+}	$5f^5$	4232.54	21.50	412.48	2821.0
Cm^{4+}	$5f^6$	4607.76	23.40	449.05	3042.0
Cm^{3+}	$5f^7$	3955.3	17.79	369.8	2876.1
Bk^{3+}	$5f^8$	4132.3	18.90	398.29	3248.5

where

$$\langle f^{n-1}(\nu'S'L')\|\, a^r \,\|f^n(\nu SL)\rangle = (-)^{r+1/2+S'+L'-S-L}\left(\frac{N(2S+1)(2L+1)}{(2S'+1)(2L'+1)}\right)^{1/2}\langle f^{n-1}S'L';r\,|\,f^nSL\rangle\,, \tag{A3}$$

and N is the number of f electrons in the initial state. The fractional parentage coefficients $\langle f^{n-1}S'L';r\,|\,f^nSL\rangle$ are tabulated by Nielson and Koster.[31] Substituting Eq. (A3) into (A2) and rearranging the equation, we obtained the relative intensity of the final-state J multiplets of the f^{n-1} configuration

$$X(\alpha'J') = NZ_f \sum_{\substack{\nu SL\\ \nu'S'L'}} (2J'+1)(2S+1)(2L+1)\left(\langle f^{n-1}\nu'S'L'J'\,|\,\alpha'J'\rangle\langle f^N\nu SLJ\,|\,\alpha J\rangle\right)^2$$
$$\times\left|\langle f^{n-1}S'L';r\,|\,f^NSL\rangle\right|^2\sum_j(2j+1)\begin{pmatrix} S & S' & \frac{1}{2}\\ L & L' & 3\\ J & J' & j\end{pmatrix}^2\,. \tag{A4}$$

The eigenvalues and eigenvectors of various $5f^n$ configurations were calculated using the Slater and spin-orbit parameters listed in Table IV. For the Cm^{3+} and Bk^{3+} ions, three more parameters, i.e., the configuration interaction parameters α, β, and γ, in addition to the Slater and spin-orbit parameters listed, were used. The parameters for the Cm^{3+} and Bk^{3+} ions were derived from spectroscopic data of Carnall and Rajnak.[32,33]

†Work supported by the U. S. Energy Research and Development Administration.

[1] *The Actinides: Electronic Structure and Related Properties*, edited by A. J. Freeman and J. B. Darby (Academic, New York, 1974).

[2] J. Verbist, J. Riga, J. J. Pireaux, and R. Caudano, J. Electron Spectrosc. Related Phenomena 5, 193 (1974).

[3] B. W. Veal and D. J. Lam, Phys. Lett. A 49, 466 (1974).

[4] B. W. Veal and D. J. Lam, Phys. Rev. B 10, 4902 (1974).

[5] T. Novakov and J. N. Hollander, Phys. Rev. B 10, 4902 (1974).

[6] M. O. Krause and F. Wuilleumier, in *Electron Spectroscopy*, edited by D. A. Shirley (North-Holland, Amsterdam, 1972), p. 759.

[7] M. O. Krause, J. R. Peterson, R. G. Haire, J. Oliver, O. Keski-Rahkonen, and J. Oliver, ORNL Report No. 5111, Oak Ridge National Laboratory, 1976 (unpublished).

[8] Y. Y. Chu, M. L. Perlman, P. F. Sittner, and C.E. Bemis, Phys. Rev. A 5, 67 (1972); J. M. Hollander, M. D. Holtz, T. Novakov, and R. L. Graham, Ark. Fys. 28, 375 (1965); I. Ahmad, F. T. Porter, M. S. Freedman, R. F. Barnes, R. K. Sjoblom, F. Wagner, Jr., J. Milsted, and P. R. Fields, Phys. Rev. B 12, 5651 (1975).

[9] J. C. Fuggle, A. F. Burr, L. M. Watson, D. J. Fabian, and W. Lang, J. Phys. F 4, 335 (1974).

[10] B. W. Veal, D. J. Lam, W. T. Carnall, and H. R. Hoekstra, Phys. Rev. B 12, 5651 (1975).

[11] F. T. Porter and M. S. Freedman (private communication).

[12] M. O. Krause, R. G. Haire, and J. H. Oliver, ORNL Report No. 5111, Oak Ridge National Laboratory, 1976 (unpublished).

[13] See, for example, (a) M. Campagna, E. Bucher, G. K. Wertheim, D. N. E. Buchanan, and L. D. Longinotti, Proceedings of the Eleventh Rare Earth Research Conference, Traverse City, Mich. Oct. 1974 (unpublished), p. 810; and (b) Y. Baer and G. Busch, J. Electron Spectrosc. Related Phenomena 5, 611 (1974).

[14] See, for example, M. Campagna, E. Bucher, G. K. Wertheim, and L. D. Longinotti, Phys. Rev. Lett. 33,

165 (1974); 32, 885 (1974).
[15]P. H. Citrin, P. Eisenberger, and D. R. Hamann, Phys. Rev. Lett. 33, 965 (1974).
[16]J. A. D. Matthew and M. G. Devey, J. Phys. C 7, L335 (1974).
[17]U. Gelius, S. Svensson, H. Siegbahn, E. Basilier, A. Faxäbu, and K. Siegbahn, Chem. Phys. Lett. 28, 1 (1974).
[18]J. Lerner, in Proceedings of the Fourth International Conference of the Nuclear Target Development Society, 29 Sept.–1 Oct. 1975, Argonne, Ill. (unpublished).
[19]E. P. Horwitz, C. A. A. Bloomquist, D. J. Henderson, and D. E. Nelson, J. Inorg. Nucl. Chem. 31, 3255 (1969).
[20]J. Hedman, Y. Baer, A. Berndtsson, M. Klasson, G. Leonhardt, R. Nilsson, and C. Nordling, J. Electron Spectrosc. Related Phenomena 1, 101 (1972/73).
[21]P. S. Bagus, A. J. Freeman, and F. Sasaki, Phys. Rev. Lett. 30, 850 (1973).
[22]S. P. Kowalczyk, N. Edelstein, F. R. McFeely, L. Ley and D. A. Shirley, Chem. Phys. Lett. 29, 491 (1974).
[23]T. A. Carlson, C. C. Lu, T. C. Tucker, C. W. Nestor, Jr., and F. B. Malik, ORNL Report No. 4614, Oak Ridge National Laboratory, 1970 (unpublished). Also see At. Data Nucl. Data Tables 3, 1 (1971).
[24]J. P. Desclaux, At. Data Nucl. Data Tables 12, 311 (1973).
[25]A. J. Freeman (private communication).
[26]V. I. Nefedov, D. Gati, B. F. Dzhurinskii, N. P. Sergushin, and Ya. V. Salyi, Zh. Neorg. Khimii 20, 2307 (1975) [Russian J. Inorg. Chem. 20, 1279 (1975)].
[27]P. A. Cox, Y. Baer, C. K. Jørgensen, Chem. Phys. Lett. 22, 433 (1973).
[28]B. G. Wybourne, J. Chem. Phys. 36, 2295 (1962).
[29]G. Racah, Phys. Rev. 61, 186 (1942).
[30]P. A. Cox, Ph.D. thesis (Oxford University, 1973) (unpublished).
[31]C. W. Nielson and G. F. Koster, *Spectroscopic Coefficients for p^n, d^n, and f^n Configurations* (MIT Press, Cambridge, Mass., 1963).
[32]W. T. Carnall and K. Rajnak, J. Chem. Phys. 63, 3510 (1975).
[33]The values for Bk^{3+} are from W. T. Carnall and F. Wagner, Jr. (private communication). The parameters were refined since the earlier work of W. T. Carnall, S. Fried, and F. Wagner, Jr., J. Chem. Phys. 58, 3614 (1973). Further refinement of the parameters is in progress [W. T. Carnall and H. Crosswhite (private communication)].